Turkish Online Journal of Qualitative Inquiry (TOJQI)
Volume 12, Issue 3, June 2021: 5026 – 5033

Research Article

Study On Fiber Gratings And Its Characterization

Dr. Ved Nath Jha* Dr. Praveen Bhatt**

Abstract

Good potential uses in fiber and fiber lasers have been seen through Random Fiber Gratings (RFGs). However, a quantitative link has never been studied between the RFG's randomness and spectral reaction. This paper first experimentally characterizes two RFGs of varying degrees of randomness by optical frequency reflectometry (OFDR). The high degree of randomness indicates that the grating intensity is limited and the strength variations in spatial domain are large. The experimental findings show. Study establishes the theoretical basis for the optimisation configuration and implementation of the long-term fiber grating in the area of fiber optics sensing and communication.

Keywords: Random, Grating, Fluctuation, Application, Characterized, Sensing,

Introduction

The new telecommunications sector has revolutionized optical fibres. Thanks to its low transmission losses, long-distance communication has become more effective. Bragg gratings (FBFs), which are in-fibre elements, have been developed after the discovery of photosensitivity in germanium-doped silicon optical fibers. FBGs are the center of optic fibers which result of exposure to extreme irradiation to a refractive index disturbance. FBGs, such as amplifiers, lasers, filters and sensors, were recently used in various forms. For sensing applications, FBGs recorded in optical fibre may be used as sensors for the calculation of physical parameters, chemical and non-specific parameters. The research would concentrate on processing and characterizing FBGs in optical fibers.

The tensile reaction arises both because the sensor is physically stretched (and the resulting shift in the grid wavelength) and because of the photoelastic effects of the fibre index.

*ASSISTANT PROFESSOR Department of Physics Mangalayatan University, Aligarh, (Uttar Pradesh)
**Associate Professor Department of Physics Himalayan University, Ita Nagar (Arunachal Pradesh)

The strain may then be characterized by the calculation of a certain location's portion of the wavelength spectrum. Owing to the effects of the rise in temperature on the caused refractory index change and, to an even lesser degree, the thermal expansion coefficient of the fibre, the FBG's temperature sensitivity arises. In addition, the measurement data is spectrally encoded to support the FBG sensors and the sensor signals are thus practically unaffected by the noise or power failure.

AFIBER Bragg grid is a typical distortion of the fibrous index induced by heart sensitivity to an intense pattern. In 1978, the creation of permanent fiber gratings was first proposed by Hill et al. at the Canadian Communications Research Center (CRC), Ottawa, ON, Canada. The intense laser radiation of argon-ion was initiated in a germanic fiber and after a few minutes the luminous strength increased until the light increased almost completely from the fiber was shown. Spectral tests, rendered indirectly by pressure and fiber grating temperature, verified the development of a very small Bragg grating filter over the whole 1-m fiber length. This accomplishment, which was then named "Hill Gratings," was an improvement in studies on the non-linear qualities of Germanic silica fiber. It noticed an unexplained fiber sensitivity, which triggered more inquiries about the origin of the photo-induced refractive behavior of the fiber and the wavelength of light used for the type of grating, many years later. Detailed studies[3] showed that the grinding force increased as the light intensity square, indicating that the mechanism was a two photon operation. In the initial tests, 488 nm laser radiation from the fiber end was mirrored, which created the grid's standing wave pattern. A single photon of half this wavelength was much more effective at 244 nm in the ultraviolet. It is seen that Meltz et al. [4] could shape gratings representing any duration of wave by illumination the fibers by side with the Manuscript obtained on 13 May 1997; and was revised on 19 May 1997. K. O. Hill is in the Middle of Communications, Ottawa, ON. The The angle between the laser and the UV wavelength, rather than visible light, was used to cladd two intersecting UV beams fired through the fiber heart, which is now the time of the disturbance limit and the index adjusts. In comparison, the forming of grating was found to be more effective in order of magnitude. Initially, photo-inducing refractiveness in fibers was then a mathematical mystery, but it became the foundation over time for a technique that now plays a significant and essential function in optical communication and sensor systems. Studies on basic processes of fiber photosensitivity and its implementation have been carried out in many European, North and South American, Asia and Australia. Some hundred photo sensitivity and fiber-grating papers were reported in science literature and in the context of topical seminars. FBGs are now easily available and in the next generation of WDM networks of large bandwidth. they find main applications in the routing, screening, monitoring and amplification of optical signals.

Literature Review

Giovanna Palumbo (2018) In this article we are discussing the specification and review for temperature measurement optimized chirped bragg grates (CFBG) sensors. In order to model CFBGs and analyze their thermal reaction, the transfer matrix technique was used. In order to understand how the thermal response CFBG differs as a function of grid design parameter and to refine the design of the particular application, the simulatory measurements were performed with various temperature profiles. Finally, a variety of computational experiments were carried out in order to evaluate the numerical simulations.

Michael Koerdt (2014) This paper focuses on the ultra violet laser-based processing and characterization of Bragg's gratings in perfluorinated optical polymer fibres. These polymer fibers display a hi-transparency relative to the traditional polymer fibres, based on polymers that are commonly most common for polymer fibers utilizing carbon hydrogen bonds such as polymethyl methacrylate. Up-to-date, only scratches recorded by the phase mask technique have been observed successfully in the thin sheets of the amorphous fluoropolymer CYTOP from

polymer fibers. For the first time in this segment infrarouge Bragg gratings are provided in perfluorinated polymer fibre.

SUNITA UGALE (2010) This paper describes models and characteristics for the optimum reflectivity of an optical fiber grating with a minimal side lobe power waste. Crucial parameter for the efficiency of fiver grating are grating duration and refractive index. With various refractive index profiles and distances, the reflective range and side lobes were studied. Apodization methods are used to maximize the scope of reflection. The simulations are based on the resolution by transfer matrix method of coupled mode equations, which explains the relationship of directed modes.

In Wei Zhang (2015), the vector terms of the center and the covering components of the electromagnetic field of long-term fibre grating are studied by using coupling mode theory. Since productive refractive indexes and the center and cladding modes have been overcome, the fibre-glazing fiber transmission range can be obtained by means of a number integration process by solving the coupling mode equations. The single-mode and multi-mode spectra of propagation was simulated. The research provides the theoretical basis for the development and application in the area of optical fibre-sensing and communication of long-term fiber grating.

Zichao Zhou (2020) When the grid's local spectral response is strong, it displays several peaks and a significant variance in wavelength. The line large of its fine frameworks reveals the comportament of scaling with the grid length. In order to find a quantitative connection between the degree of randomity and the continuum properties, Entropy was implemented to describe the level of randomness produced by changing the sub-grid era. The simulation results showed that the average RFG reflectivity of dB size was linearly decreased when the measured range of subgrid wavelengths was smaller than the total range of spectrum deviations. The highest R FG reflectivity was determined by¨2L àP (where¨is the coupling coefficient, L is the length of the grid and¨äP is the time of the subcoupling transition) and not¨l if¨äP is more than 8 nm in the area of space. The results of these tests align well with simulation results that enable RFG processes for future random laser and sensor applications to be refined.

Bragg grating generation

A laser with an unreliable resonator was using Lambda Physik LPX 305i. The profile of the laser beam was lowered by aperture to 1 cm · 1 cm. The pulse fluence was modified by a machine operated external attenuator inserted into the radiation route and stabilized throughout the irradiation phase. In order to do this, a constant 10 percent pulse energy was separated to a calibrated sensor such that this portion of each pulse energy was captured during radiation experiments. When the predefined total fluence was attained, the laser was immediately shut off. The Bragg gratings were produced by the technique of a phase mask. One end of the As outlined in the adhesive figure, samples were fixed to the combined sample- and phase-mask holder. The holder is an aluminum plate with a hole and many boundary guides. The gap led to the laser beam. The rim guides and mechanical stops have led to the POF fitting of the mask. A glass plate of around 2 grams and adhesive was added to the other end of the fiber to enable adequate friction on the side of the holder. This can be seen in the retain the strong and straight fiber. The ± 1-phase mask, optimized for 248 nm, was acquired from Ibsen Photonics A/S, Denmark. The 1084.45 nm grid surface area is 1 cm · 2 cm long. The phase mask was associated with the grid

side in direct contact with the sample of the stationary polymer optical fiber, so that the grating streams were perpendicular to the longitudinal fiber direction. Parallel to the longer dimension of the UV cross beam the mask grid was aligned with its striations.

Experimental Characterization of RFG

Figure 1 demonstrates the configuration of RFG characterization. An extra interferometer, an interferometer, and an optical receiving system were used in the optical system. With an optical beatswave, which is used to enable the signal sampling from the measurement interferometer at the same period of the wave length is produced in a tunable laser that sweats its output frequency linearly. The tunable light is lit up in two arms in the measuring interferometer. The beat signal is then captured and sent by the photodetector, the original accurate signal we get from the OF DR setup in the wavelength domain, to the analog Digital Conversion Device (ADC) system. On the right side of Figure 1 is shown the data processing system used to classify the RFG. The first approach to measure a complicated data collection that includes the amplitude and the reflexibility step is to quickly convert the Fourier (FFT) of the initial re-evaluated signal in the wavelength domain. The reflectivity of RFG is then accomplished by taking the module of a dynamic signal inside the space field at various locations. In addition, for further analysing, an FFT is added to the reflectivity Module to analyze the reflectivity properties of RFG throughout the spatial domain. Simultaneously a fitting window is used to translate the signal into its domain of wavelength for the dynamic data inside the space domain with inverse FFT (IFFT). The restored data in the wavelength domain is another dynamic data collection that displays the local spectral reaction of the chosen sites of the RFG with its modulus. Another FFT measurement is used to evaluate the fine spectral reaction structures of the RFG.

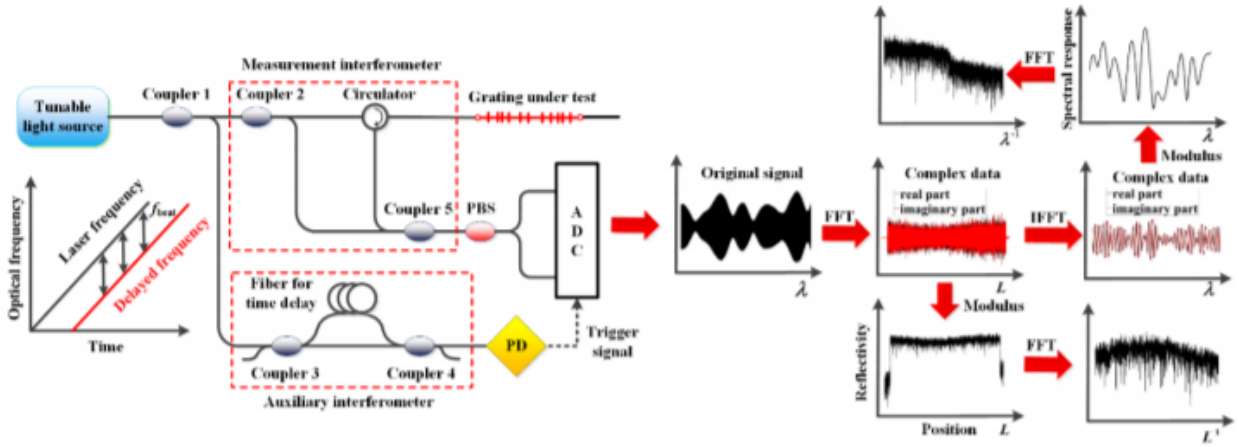

Figure 1. Experiment setup for RFG characterization and data processing method

Two RFGs with separate variations of the subgrid duration were characterized in the experiment. A femtosecond laser of the same pulse energy and containing a significant number of uniform subgratings was etched on both RFGs. Every subgrid was around 0.025 mm long and each grid's total length was about 50 mm. The discrepancy was the spontaneous distribution of the substrates during the first RFG from the 0,5328 to the 0,5436 μm range of 10,8 nm, which is far lower than the optical 1.5 micronutritional wavelength. In the second RFG, each subgrade was assigned from 0 to 2,5 μm randomly. The different size of the fluctuation of the RFG random

intervals results in different randomness amounts in the fiber media. The randomness degree represents the machine dysfunction.

Several techniques have been used to prove the presence of Bragg filament. In order to verify the grating composition, the radiated fiber samples were studied by optical microscopy. Jenapol, type Interphako, designed the microscope. A VHX-1000 with a VH-100UR was used for the microphotograph. The beams diffracted by grating is described by a laser-based diffraction setup. With a diameter of 1 mm, the red (O = 633 nm) helium neon ray is perpendicular to the polymer fiber axis and hits the polymer optical fiber in a grating-zone where the fibers are radiated with the UV crypton excimer laser. In the diffraction tests, the fiber was placed on an allocation holder for precise alignment of the samples. The diffracted beams of the produced grating were visualized with a screen with a split consisting of two white papers. The zero-beam order was guided through the slit so that only diffracted beams and inevitable street light illuminate the panel.

Transmission spectrum for the LPFG

Figure 1(a) indicates the scope of the transmission for the link to the 7th mode of the core mode. In addition to the maximum Resonance peak at μ=1562nm, on both sides of the maximum Resonance peak several minor Resonance peaks occur. The mutations of the fiber main refractive index on both ends of the fiber induce these sidelobes. These sidelobes have far fewer energies than the μ=1 562 nm resonance max, so they can be usually ignored. Figure 2(b) demonstrates the spectrum propagation of the LPFG with the multi-reclad mode orders for key mode connections. We can see that in the transmitting range a variety of distinct loss peaks occur. Any loss peak represents a peculiar number cladding mode with the core mode, and the loss peaks with equivalent number cladding modes which are referring to the core mode are so tiny that they are almost invisible to our eyes. With the rise of the cladding mode the distances between neighboring failure peaks and transmissivities increase. The explanation is that part of the energy correlated with the reinforcement modes is re-connected to the corn mode, meaning that reinforcing the reinforcement mode reduces easily. In comparison, the binding power is very poor for higher order cladding modes, which makes the loss peaks so tiny that the propagation range cannot be detected.

Single-mode fiber sensors have a greater sensitivity, enabling the consumer to directly create directed wave interferometers from the fiber itself to quantify minor phase differences in light transmitted through the measurement area. The relation of the process of the light wave that travels through a sensing path is rendered with the stage of another light wave that comes from the same source. The phase variation will then be calculated at a sensitivity of ~10-6 wavelengths when the path duration will be millions of wavelengths for the measuring relationship. The optical direction of one in 1012 could therefore be calculated with a potential resolution. Around the same time, the lack of space-free optical pathways between origins and detectors prevents sluggish alignment drifts that might easily arise in case of a bulk optic interferometer. In reality, single-mode fiber sensors need very robust, very reliable, low-phase noise sources so their potential sensitivity can be completely taken advantage of. If such sources are used, it is usually not necessary to calibrate the phase difference, and the interferometer output is periodized in its design.

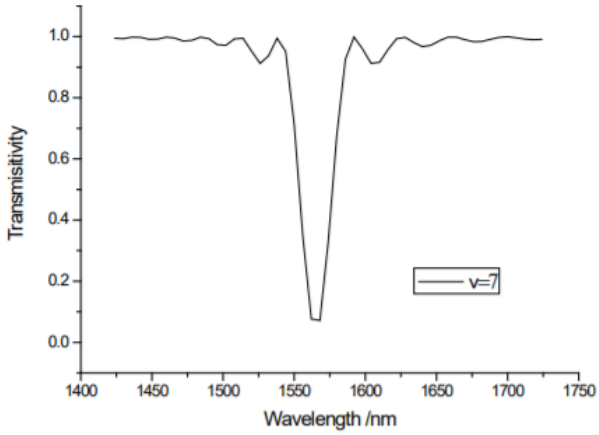

(a) Single Mode

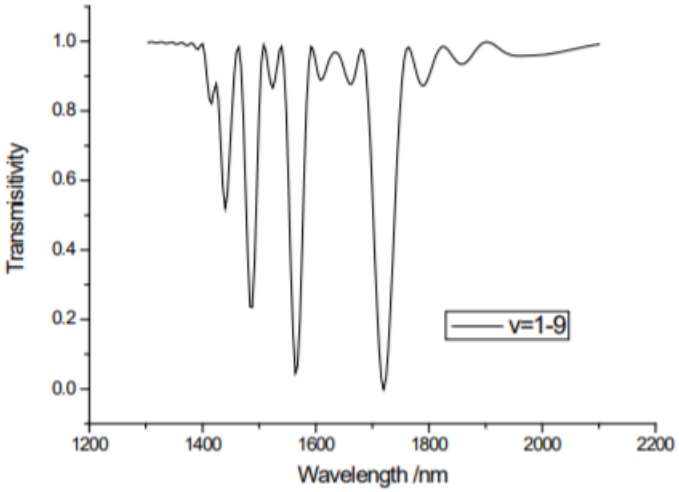

(b) Multiple Mode

As in table 1 the reflectivity of Standardized FBG varies for various grid lengths, with the rise in grid duration and the variation in the index. 100 percent reflectivity is reached almost after a lenght of 2,5 mm. With increased grid duration and index variations, the resistance of the side lobes in reflectivity curve uniform FBG is increased. Different index profiles, called modification, will reduce the energy expended in side lobes.

Table 1. Dependence of reflectivity on grating length and index difference

FBG	**Δn0:0.01 Λ = 0.5319**	**Δn0:0.008 Λ= 0.5325**	**Δn0:0.05 Λ=0.5334**	**Δn0:0.03 Λ= 0.5339**
Lmm	R	R	R	R
0.5	62.40%	50.42%	53.67%	42.85%
1	92.56%	85.67%	80.70%	82.12%
1.5	98.46%	98.14%	96.45%	93.32%
2	100%	100%	99.87%	99.01%

2.5	100%	100%	100%	100%
5	100%	100%	100%	100%
10	100%	100%	100%	100%
20	100%	100%	100%	100%

Conclusion

This analysis was focused on the system of transfer matrix and was defined by the OFDR method of reflectivity and spectral properties of RFGs. Second, the effects of the randomness to the diluted grid intensity and spectral reaction properties can be experimentally evaluated qualitatively by contrasting the various characteristics of low and higher disordered RFGs. Higher randomness levels of RFG result in lower light diffuse intensities and greater spatial domain intensity variability. The low randomness results in a particular rate fluctuation duration for low-disordered RFGs. A high level of randomness results in rich fine structures and a broader spectrum of wavelength fluctuations for local spectral reaction. The linewidths of the RFG's fine spectral properties are scalable and lengthy. It analyses and measures the propagation range of the long distance fiber gratings At first, fiber core and cladding electrical and magnetic fields are measured by means of vector processing, the fibre core, cladding, film and exterior atmosphere components are computed. And the coupling constant and the powerful fiber core and cover mode refractive index are obtained. Finally, by combining the coupling-mode equations, the amplitude of the fiber core and the cladding mode are measured and the propagation of the long-term galvanization is accomplished. The study will include some theory to refine the architecture and practical implementation of the long-term fiber grating in the field of optical fibre communication.

References

1. Giovanna Palumbo, Analysis and Design of Chirped Fiber Bragg Grating for Temperature Sensing for Possible Biomedical Applications, IEEE Photonics Journal, 2018

2. Kenneth O. Hill and Gerald Meltz, Fiber Bragg Grating Technology Fundamentals and Overview, JOURNAL OF LIGHTWAVE TECHNOLOGY, VOL. 15, NO. 8, AUGUST 1997

3. Michael Koerdt, Fabrication and characterization of Bragg gratings in a graded-index perfluorinated polymer optical fiber, Procedia Technology 15 (2014) 138 – 146

4. **Skaar, Johannes. (2000). Synthesis and characterization of fiber Bragg gratings.**

5. **Ugale, Sunita & Mishra, Vivekanand. (2010). Fiber Bragg Grating Modeling, Characterization and Optimization with different index profiles. International Journal of Engineering Science and Technology. 2.**

6. Wei Zhang, Calculation of the Transmission Spectrum of Long-Period Fiber Grating Based on the Mode Field Analysis Method, International Symposium on Computers & Informatics (ISCI 2015)

7. Zichao Zhou, Random Fiber Grating Characterization Based on OFDR and Transfer Matrix Method, Sensors 2020, 20, 6071

8. J.-J. Liau, A NEW LOOK AT NUMERICAL ANALYSIS OF UNIFORM FIBER BRAGG GRATINGS USING COUPLED MODE THEORY, Progress In Electromagnetics Research, PIER 93, 385–401, 2009

9. Abdullina, S.; Skvortsov, M.; Vlasov, A.; Podivilov, E.; Babin, S. Coherent Raman lasing in a short polarization-maintaining fiber with a random fiber Bragg grating array. Laser Phys. Lett. 2019, 16, 105001.

10. Chiavaioli, F.; Baldini, F.; Trono, C. Manufacturing and spectral features of different types of long period fiber gratings: Phase-shifted, turn-around point, internally tilted, and pseudo-random. Fibers 2017, 5, 29.

11. Lizárraga, N.; Puente, N.; Chaikina, E.; Leskova, T.; Méndez, E. Single-mode Er-doped fiber random laser with distributed Bragg grating feedback. Opt. Express 2009, 17, 395–404.

12. Gagné, M.; Kashyap, R. Demonstration of a 3 mW threshold Er-doped random fiber laser based on a unique fiber Bragg grating. Opt. Express 2009, 17, 19067–19074.

13. Xu, Y.; Lu, P.; Gao, S.; Xiang, D.; Lu, P.; Mihailov, S.; Bao, X. Optical fiber random grating-based multiparameter sensor. Opt. Lett. 2015, 40, 5514–5517.

14. Li, Y.; Lu, P.; Bao, X.; Ou, Z. Random spaced index modulation for a narrow linewidth tunable fiber laser with low intensity noise. Opt. Lett. 2014, 39, 2294–2297

15. Monet, F.; Loranger, S.; Lambin-Iezzi, V.; Drouin, A.; Kadoury, S.; Kashyap, R. The ROGUE: A novel, noise-generated random grating. Opt. Express 2019, 27, 13895–13909.